Desalination and Water Treatment
www.deswater.com
doi: 10.1080/19443994.2013.830690

52 (2014) 7660–7672
December

Taylor & Francis
Taylor & Francis Group

Synthesis and characterization of an inorganic/organic-modified bentonite and its application in methyl orange water treatment

Jing Wang[a], Hongzhu Ma[a,*], Wenfeng Yuan[a], Wenyan He[a], Shanshan Wang[a], Jing You[b]

[a]*School of Chemistry and Chemical Engineering, Institute of Energy Chemistry, Shaanxi Normal University, Xi'an 710062, China*
Tel. +86 29 81530726; Fax: +86 29 81530727; email: hzmachem@snnu.edu.cn
[b]*State Key Laboratory of Organic Geochemistry, Guangzhou Institute of Geochemistry, Chinese Academy of Sciences, Guangzhou 510640, China*

Received 3 March 2012; Accepted 23 July 2013

ABSTRACT

The adsorption of methyl orange (MO) onto hydroxyl-aluminum and cetyltrimethyl ammonium bromide (CTAB)-modified bentonite (Al/CTAB-bent) was studied. The effects of contact time, Al/CTAB-bent dosage, temperature, initial pH and an initial MO concentration on MO adsorption were investigated. The surface properties and structure of Al/CTAB-bent were measured by some techniques, such as X-ray diffraction, scanning electron microscope, Brunauer–Emmett–Teller, energy dispersive X-ray spectroscopy and Fourier transform infrared spectrometry. The color and chemical oxygen demand removal efficiency can reach up to 99% and 97%, respectively. The adsorption kinetics and isotherm of MO onto Al/CTAB-bent were also investigated. The results revealed that Langmuir model was more suitable to describe MO adsorption than Freundlich model. The adsorption kinetics follows the pseudo-second-order kinetics model better. The thermodynamic parameters such as ΔG_0, ΔH_0, and ΔS_0 were also evaluated.

Keywords: Bentonite; Al/CTAB-bent; Methyl orange; Adsorption isotherm; Adsorption kinetics

1. Introduction

Large amounts of dyes discharged by textile industries can be very toxic even at a very low concentration [1,2]. Various methods have been developed for the treatment of color dyes [3–8], and as an effective method for contaminant treatment, adsorption appears to offer the best potential for color removal. Activated carbon is one of the most widely used adsorbents for removing dyes from aqueous solutions [9], but it is limited due to its high operation costs. Many low-cost adsorbents, such as hen feather [10], Oedogonium [11], bagasse fly ash [12], activated carbon developed from thermal and chemical treatment of waste rubber tire [13,14], bottom ash and deoiled soya [15–18], carbon slurry [19,20], deoiled mustard [21], adsorbent prepared from orange peel and Fe_2O_3 nanoparticles [22], wheat husk [23], bentonite and kaolinite [24,25], are being developed. Clays are one of the most widely used low-cost minerals due to their abundant availability [26].

*Corresponding author.

Bentonite, mainly composed of montmorillonite, with a 2:1-type aluminosilicate, consists of one $A1^{3+}$ octahedral sheet placed between two Si^{4+} tetrahedral sheets in a unit. Its surface is negatively charged due to isomorphous substitution of Al^{3+} for Si^{4+} in the tetrahedral layer and Mg^{2+} for Al^{3+} in the octahedral layer. This negative charge is balanced by exchangeable cations such as Na^{+} or Ca^{2+} in lattice structure. Na^{+} and Ca^{2+} hydrate in the presence of water; therefore, the clay surface is hydrophilic and raw bentonite is not an effective adsorbent for the non-polar organic compounds in water [27]. When the cations (Na^{+}, Ca^{2+}) in the bentonite layer were replaced by inorganic hydroxyl-metal polycations, they act as pillars and increase the interlayer spacing of bentonite and then improve the adsorptive capacity for organic compounds. The organo-bentonite has strong affinity for organic compounds and so is widely used in wastewater treatment; but, important disadvantage is that it difficult to separate the organo-bentonite from the treated water [28].

In this investigation, an inorganic/organic-modified bentonite, Al/CTAB-bent, was synthesized by intercalating bentonite with cetyltrimethyl ammonium bromide (CTAB) and hydroxy-aluminum (Al_{13}), and characterized by X-ray diffraction (XRD), scanning electron microscope (SEM), Brunauer–Emmett–Teller (BET), energy dispersive X-ray spectroscopy (EDXS) and Fourier transform infrared (FTIR) spectrometry. The investigation on methyl orange (MO) removal was carried out by a series of batch adsorption experiments. More attention has been paid on the understanding of the kinetics, thermodynamics and equilibrium processes involved in the adsorption of MO onto Al/CTAB-bent. The effects of contact time, initial pH, MO initial concentration and temperature on the adsorption phenomena have also been studied.

Table 1
The laboratory instruments

Instrument	Model	Company
pH meter		
UV-vis	UV-7504	Persee Instrument co., Ltd., Beijing, China
COD meter		
FTIR	Tensor27	Brucher instrument co., Ltd., Germany
X-ray diffractometer	D/Max-3c	Rigaku Corporation, Japan

2. Experimental section

2.1. Materials and instrument

The laboratory instruments are shown in Table 1.

MO obtained from Tianjin, China, was used as received without any further purification. The raw bentonite supplied by Henan, China, was dried at 353 K in a laboratory oven to constant mass before using it. CTAB obtained from Tianjin, China, and $Al_2(SO_4)_3$ and NaOH obtained from Chengdu, China, are of analytical grade and used without further purification.

2.2. Preparation of Al-bent and Al/CTAB-bent

Al-bent was prepared by dispersing 20 g of Na-bentonite (Na-bent) in 400 mL of distilled water, followed by an addition of 500 mL of a dispersion of aluminum hydroxide in dropwise, which was prepared by adding 0.48 mol L^{-1} of NaOH solution slowly to 0.1 mol L^{-1} $Al_2(SO_4)_3$ solution under vigorous stirring for 24 h at 353 K, until the OH^{-}/Al^{3+} molar ratio of 2.4 was obtained. The resulting dispersion was stirred and heated for 12 h at 333 K. Then, the slurry was washed with deionized water for several times. The solid was dried at 353 K to constant mass, activated for 1 h at 413 K, ground and stored in air-tight plastic bottles in a desiccator for further use.

Al/CTAB-bent was prepared by adding a certain amount of CTAB solution to a 2% aqueous suspension of 20 g of Al-bent under stirring. The suspension was heated for 3 h at 313 K, collected by filtration, washed, dried at 353 K to constant mass, activated for 1 h at 413 K, ground and stored in air-tight plastic bottles in a desiccator for further use.

2.3. Characterization of Al/CTAB-bent

The samples were analyzed by XRD using a Rigaku apparatus with Cu Kα radiation. The XRD of the raw bentonite, Al-bent, and Al/CTAB-bent sample was detected and the mineral components presented in the samples were identified using JCPDS data files. SEM measurements were performed using a Quanta 200 SEM produced by Philips at 20 kV. To determine the component and atomic ratios in the adsorbents along the surface cross-section, the signal of surface elements was detected by EDXS mapping method. The BET-specific area and pore structure of adsorbent were obtained from nitrogen adsorption data at 77 K using a Micromeritics ASAP2020 system. Prior to analyses, the samples were degassed at 383 K for 4 h under vacuum conditions. FT-IR spectra of the samples with KBr pellet were recorded in the spectrum range of 4,000–500 cm^{-1} on a FT-IR spectrometer.

2.4. Adsorption experiments

Adsorption of MO on bentonite was carried out in a batch system. A 100 mL MO solution (100–300 mgL^{-1}) in the conical flasks was stirred at 150 rpm at room temperature. During each run, the samples were withdrawn at regular time intervals, centrifuged for 4 min to separate the dye solution from the adsorbent, and evaluated for the color and chemical oxygen demand (COD) removal efficiencies. All adsorption trials and sample tests were carried out in triplicates.

2.5. Analysis and calculation

MO concentration was determined by UV–visible spectrophotometer with quartz cell (1 cm path length) at 466 nm. The COD values were measured by COD meter. The adsorption capacity q_t, color and COD removal efficiency of MO were calculated from the equations:

$$q_t = \frac{(c_0 - c_t)V}{W} \quad (1)$$

$$\text{Color removal efficiency}(\%) = \frac{A_0 - A_t}{A_0} \times 100\% \quad (2)$$

$$\text{COD removal efficiency}(\%) = \frac{\text{COD}_0 - \text{COD}_t}{\text{COD}_0} \times 100\% \quad (3)$$

where q_t (mg g^{-1}) is the amount of MO dye adsorbed per unit mass of adsorbent; c_0 (mg L^{-1}) and c_t (mg L^{-1}) are MO concentrations at initial and time t; V (L) is the volume of solution; and W (g) is the mass of the adsorbent. A_0 is the initial absorbance of MO at 466 nm; A_t is the absorbance of MO at time t at 466 nm; COD_0 is the initial COD value of MO; and COD_t is the COD value of MO at time t.

2.6. Adsorption kinetics

In order to understand the mechanisms and dynamics of the adsorption process, experimental data generated from MO adsorption tests were evaluated by pseudo-first-order and pseudo-second-order kinetics.

The Lagergren pseudo-first-order model is given by Eq. (4) [29]:

$$\log(q_e - q_t) = \log q_e - \frac{k_1}{2.303}t \quad (4)$$

where q_t (mg g^{-1}) is the adsorption capacity at time t; q_e (mg g^{-1}) is the adsorption capacity at equilibrium; and k_1 (min^{-1}) represents the rate constant of the pseudo-first-order model.

The pseudo-second-order [30] equation is defined as follows:

$$\frac{t}{q_t} = \frac{1}{k_2 q_e^2} + \frac{t}{q_e} \quad (5)$$

where k_2 (L mg^{-1} min^{-1}) is the rate constant of the pseudo-second-order model.

2.7. Adsorption isotherm

Adsorption isotherm is the equilibrium relationship between the concentration in the liquid phase and the concentration in the adsorbent phase on the adsorbent particles at a given temperature [31,32]. The experimental data to describe the adsorption of MO dye on Al/CTAB-bent are analyzed by Langmuir, Freundlich, and Temkin isotherms.

Langmuir model is based on three following assumptions [33]: (1) the adsorption of molecule is a monolayer adsorption; (2) the adsorbent surface is uniform; and (3) there is no interaction among the adsorbed molecules. The Freundlich model is generally found to be better fit for characterizing multi-layer adsorption process than the Langmuir model [34]. Temkin isotherm [35] assumes that decrease in the heat of adsorption is linear and the adsorption is characterized by a uniform distribution of binding energies.

The Langmuir isotherm can be expressed as Eq. (6) or Eq. (7):

$$q_e = \frac{q_m K_L c_e}{1 + K_L} \quad (6)$$

$$\frac{c_e}{q_e} = \frac{1}{q_m K_L} + \frac{c_e}{q_m} \quad (7)$$

where c_e is the equilibrium concentration of adsorbates in the solution (mg L^{-1}); q_e is the equilibrium adsorption amount (mg g^{-1}); q_m is the monolayer adsorption capacity (mg g^{-1}); and K_L is the Langmuir adsorption equilibrium constant (L mg^{-1}). The q_m and K_L can be determined by the intercept and the slope of the linear plot of c_e/q_e vs. c_e, respectively.

Freundlich equation can be expressed as Eq. (8):

$$q_e = K_F c_e^{1/n} \quad (8)$$

where q_e is the equilibrium adsorption amount of adsorbates ($mg\,g^{-1}$); K_F is the Freundlich adsorption equilibrium constant ($(mg\,g^{-1})(mg\,L^{-1})^n$); c_e is the equilibrium concentration of adsorbates in the solution ($mg\,L^{-1}$); 1/n is the heterogeneity factor. Eq. (8) can be rearranged in a linear form as Eq. (9). K_F can be determined by the intercept of $\ln q_e$ vs. $\ln c_e$.

$$\log q_e = \log K_F + \frac{1}{n} \log c_e \quad (9)$$

Temkin isotherm can be expressed as Eq. (10).

$$q_e = A + B \ln c_e \quad (10)$$

where $B = RT/b$, b is a constant about adsorption heat ($J\,mol^{-1}$), A is the Temkin constant (Lg^{-1}), R is the gas constant ($8.314\,J\,mol^{-1}\,K^{-1}$), and T is the temperature (K). The A and B can be determined by the intercept and the slope of the linear plot of q_e vs. $\ln c_e$, respectively.

2.8. Thermodynamic studies

The thermodynamic parameters, such as Gibbs free-energy changes ΔG_0, standard enthalpy changes ΔH_0, and standard entropy changes ΔS_0, were also studied to better understand the adsorption mechanism.

The Gibbs free-energy changes ΔG_0 were calculated by Eq. (11):

$$\Delta G_0 = -RT \ln K_C \quad (11)$$

Standard enthalpy changes, ΔH_0, and standard entropy changes, ΔS_0, were calculated by Eq. (12):

$$\ln K_C = -\frac{\Delta H_0}{RT} + \frac{\Delta S_0}{R} \quad (12)$$

Adsorption equilibrium constant K_c value was calculated by Eq. (13):

$$K_C = \frac{c_{AE}}{c_{SE}} \quad (13)$$

c_{AE} is the amount of dye (mg) adsorbed on the adsorbent per L of the solution at equilibrium. c_{SE} is the equilibrium concentration ($mg\,L^{-1}$) of the dye in the solution.

3. Results and discussion

3.1. Characterization of Al/CTAB-bent

XRD analysis was carried out in order to identify the mineralogical structure of the modified bentonite adsorbents and the XRD patterns are shown in Fig. 1. It can be seen that similar diffraction peaks owing to the complex components of adsorbents were detected in these three samples. The main crystalline phases observed in raw-bent for SiO_2, observed at 2θ of 6.61°, 19.60°, 21.69°, 26.69°, 36.71° and 62.04°, which were in line with that of the literature reported [36]. The increase of basal spacing from 13.26 Å for raw-bent to 17.25 Å for Al/CTAB-bent was due to the intercalation of Al and CTAB molecule onto the interlayer space of raw-bent which expanded its interlamellar spacing and later promoted MO adsorption capacity, which was also confirmed by FT-IR.

SEM images of the adsorbents are presented in Fig. 2. Although it was not possible to exactly determine the particle size of the adsorbents, large aggregates of platelets mixed with small particles, mainly between 10 and 30 μm in size, and were observed for the raw bentonite. After modification, the average particle size decreases, small and well-separated particles could be observed, especially for Al/CTAB-bent. The particles appear more compacted, even though it is not possible to see if they are still porous or not. This observation suggested that some disaggregation of bentonite particles was occurred during the modification.

The EDXS patterns of Al/CTAB-bent and its analysis are given in Fig. 3. It is obviously observed that raw-bent (Fig. 2(A)) showed distinct peaks for Si, O, Na, Al, Mg, Ca and Fe while after modifying with

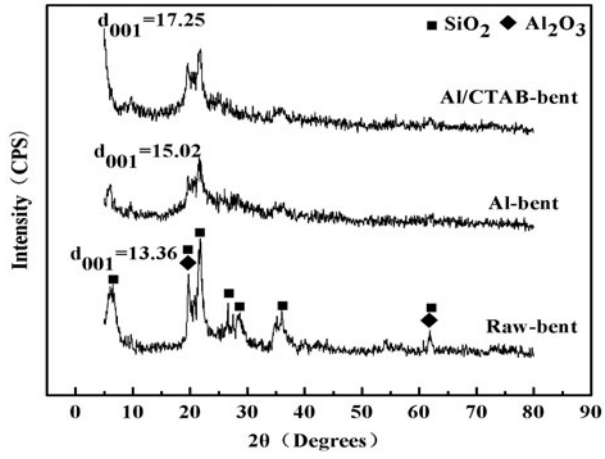

Fig. 1. XRD patterns of the adsorbents.

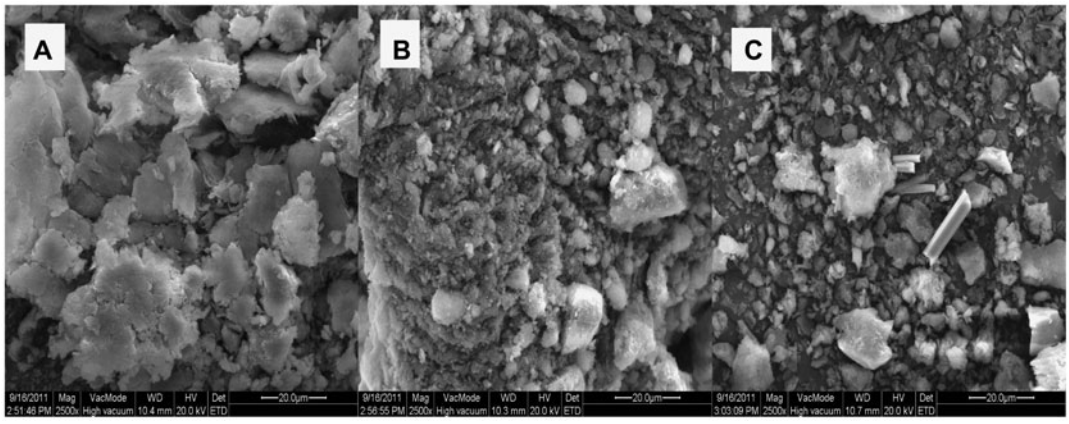

Fig. 2. SEM images of the adsorbents. (A) raw-bent; (B) Al-bent; and (C) Al/CTAB-bent.

Al_{13} and CTAB (Fig. 2(B)–2(C)), the peak of Al was increased, indicating that the successful modification.

BET surface area and the pore diameter of Al/CTAB-bent in this study are displayed in Table 2. The specific area of raw-bent, Al-bent and Al/CTAB-bent was determined as 21.65, 26.74, and 56.59 $m^2 g^{-1}$, respectively; a significant increasing in specific area for Al/CTAB-bent was observed. A major increasing in the pore diameter could be observed when Al_{13} was introduced into the raw bentonite, while a minor decreasing was observed when Al_{13} and CTAB were introduced simultaneously. However, the pore volume shows an increasing trend with Al_{13} and CTAB modifications. It was also supported by the results of pore size distributions presented in Fig. 4. The pore size distribution indicated that the mesoporous (2–50 nm) and the macroporous (50–100 nm) structures were existed in raw-bent, Al-bent, and Al/CTAB-bent, suggesting that the adsorption can be carried out with high removal efficiency, which was in line with the experiment results. These results also indicate that raw bentonite was successfully modified with Al and CTAB.

The FT-IR spectra of raw bentonite, Al-bent, and Al/CTAB-bent in the range of 4,000–500 cm^{-1} are shown in Fig. 5. The band at around 1,036 cm^{-1} can be assigned to Si–O stretching vibrations. The Si–O–Al and Si–O–Si bending vibrations appeared at 519 and 467 cm^{-1}, respectively. The bands at 3,448, 3,625 and 1,643 cm^{-1}, assigned to the OH deformation of water, were observed in the raw bentonite, Al-bent, and Al/CTAB-bent, while the peak intensity of Al/CTAB-bent was lower than that of raw-bent and Al-bent. It can also be found that the bands of Al/CTAB-bent at 2,923 and 2,852 cm^{-1} were correspond to the CH_2 asymmetric stretching mode ($v_{as}(CH_2)$) and the symmetric stretching mode ($v_s(CH_2)$), respectively[37], indicating that CTAB molecules were impregnated onto the bentonite and the increase of the hydrophobic nature of the bentonite surface after CTAB modification [38].

3.2. Effect of various parameters on MO removal

3.2.1. Comparison of different adsorbents

Blank experiment was carried out at the optimum conditions (adsorbent dosage: 0.5 g, temperature: 293 K, pH > 3, and MO concentration: 100 mg L^{-1}). It can be found that the color removal efficiency (Fig. 6) and COD removal efficiency (Table 3) for Al/CTAB-bent were high up to 99 and 97% at 30 min respectively, higher than those of raw-bent and Al-bent. This maybe due to that the surface of raw-bent is negatively charged, that is balanced by exchangeable cations such as Na^+ or Ca^{2+} hydrated in the presence of water in lattice structure, so the raw-bent is not an effective adsorbent for the organic compounds in water. Al/CTAB-bent was used in the further studies.

3.2.2. Influence of contact time

In the same adsorption conditions: Al/CTAB-bent dosage: 0.5 g, temperature: 293 K, pH > 3, and MO concentration: 100 mg L^{-1}, the influence of contact time (0–100 min) on the color and COD removal efficiency of MO was investigated. It is found from Fig. 7 that the color removal efficiency increased rapidly to 97.8% at the initial 5 min, while the maximum adsorption was obtained at 30 min, and the final color removal efficiency and COD removal efficiency were higher than 99 and 98% respectively. The color and COD removal was almost unchanged with sequentially increasing the contact time,

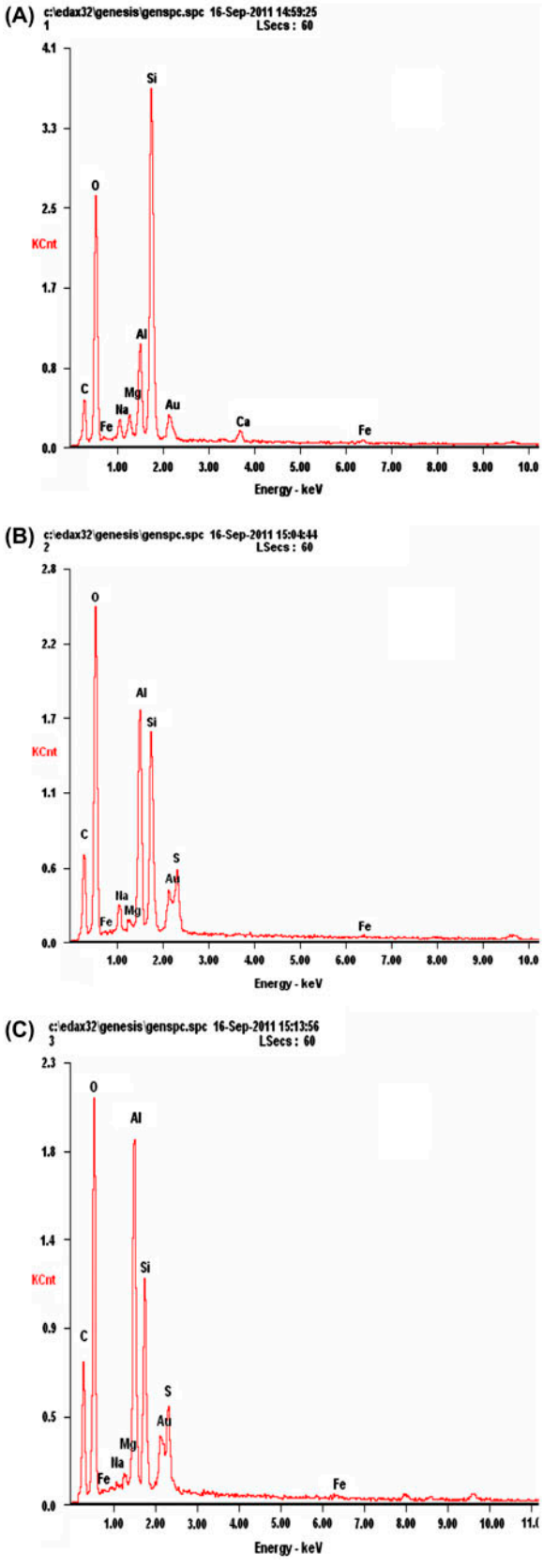

Fig. 3. EDX patterns of the adsorbents. (A) raw-bent; (B) Al-bent; and (C) Al/CTAB-bent.

indicating that the adsorption process is rapid and reachs the equilibrium, that is consistent with reference reported [39,40]. This reason may be ascribed as follows: a high concentration gradient existed between the bulk solution and the adsorbent at the early adsorption period due to the availability of a large number of vacant sites, which acts as a driving force to transfer dye molecules from bulk solution to the adsorbent surface [41]. The optimum contact time was chosen as 30 min.

3.2.3. Effect of the amount of Al/CTAB-bent

In the same adsorption conditions: temperature: 293 K, pH > 3, MO concentration: 100 mg L^{-1}, and contact time: 30 min, the Al/CTAB-bent dosage (0.3–0.7 g) on the color and COD removal efficiency of MO was investigated.

The effect of Al/CTAB-bent dosage on the color removal is shown in Fig. 8. It was found that the removal of MO increased with the increasing amount of Al/CTAB-bent. However, it is not necessary to use a much higher Al/CTAB-bent dosage because the removal efficiency was rather constant as the Al/CTAB-bent dosage increased to a certain degree. When Al/CTAB-bent was 0.5 g, the color removal efficiency of MO was up to 99%, so this amount of Al/CTAB-bent was used for further experiments.

3.2.4. Effect of initial pH on adsorption

Depending on pH, MO has two different chemical structure; quinoid that is a main form at low pH and

Table 2
Surface parameters of raw-bent, Al-bent, and Al/CTAB-bent

Sample	BET surface area (m^2g^{-1})[a]	Pore diameter by BJH (nm)[b]	Pore volume (cm^3g^{-1})[c]
Raw-bent	21.65	82.13	0.0484
Al-bent	26.74	143.47	0.0768
Al/CTAB-bent	56.59	68.29	0.107

Notes: [a]BET surface area calculated from the linear part of the BET plot ($p/p_0 = 0.2$).[b]Average pore diameter, estimated using the desorption branch of the isotherm and the Barrett–Joyner–Halenda (BJH) formula.[c]Total pore volume, taken from the volume of N_2 adsorbed at $p/p_0 = 0.971$.

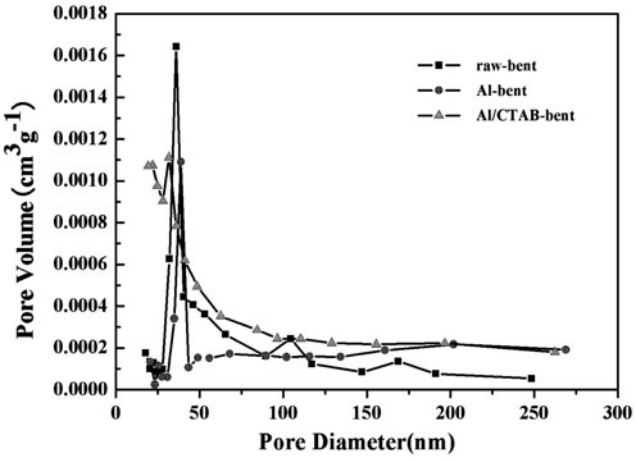

Fig. 4. The pore size distributions of the adsorbents.

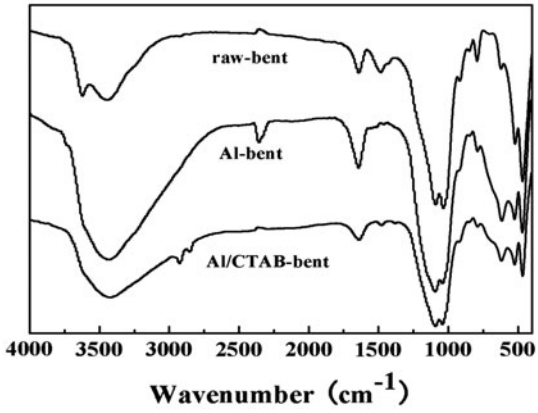

Fig. 5. FT-IR spectra of the adsorbents.

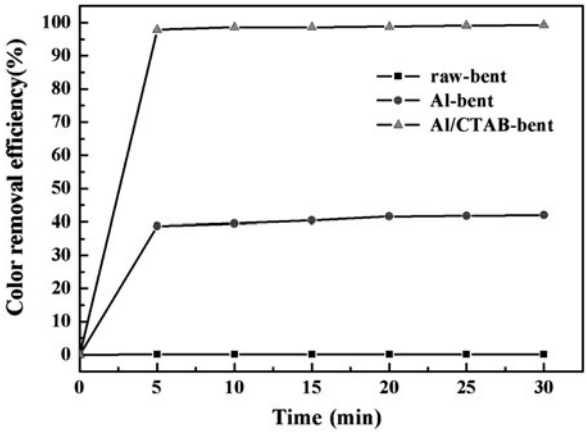

Fig. 6. Comparison of the three adsorbents on color removal efficiency (adsorbent dosage: 0.5 g, temperature: 293 K, pH > 3, and MO concentration: 100 mgL^{-1}).

Table 3
Comparison of the three adsorbents on COD removal

Adsorbent	COD removal (%)
Raw-bent	0
Al-bent	50.32
Al/CTAB-bent	97.89

Notes: Adsorbent dosage: 0.5 g, temperature: 293 K, pH > 3, and MO concentration: 100 mgL^{-1}.

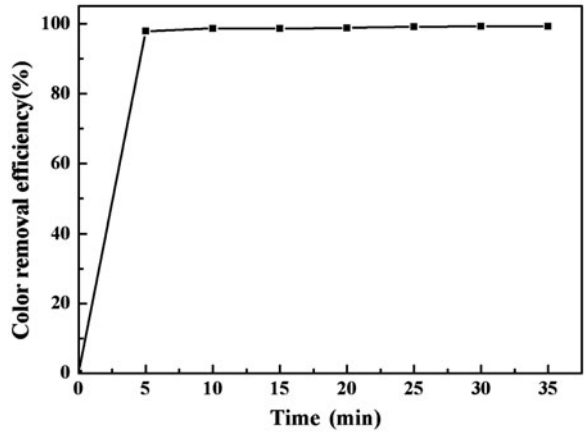

Fig. 7. Effect of contact time on color removal efficiency.

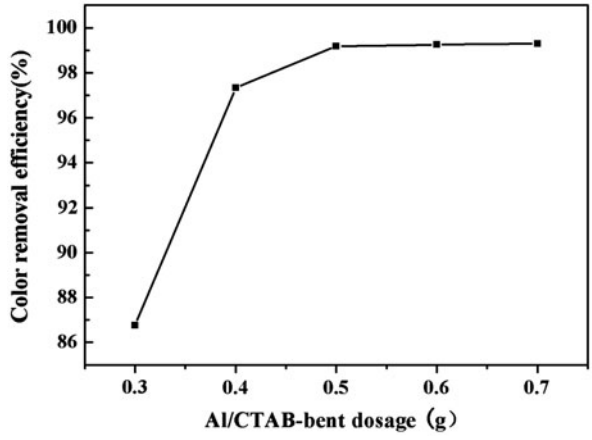

Fig. 8. Effect of adsorbent dosage on color removal efficiency.

azo at high pH [42], as shown in Fig. 9. Under the same conditions, the influence of pH (1, 3, 5, 7, 9, 11, 13, and 14) on the color and COD removal efficiency of MO was investigated and is shown in Fig. 10. The results show that color removal efficiency increased from 82.44 to 99.79%, as the pH increased from 1 to 3.

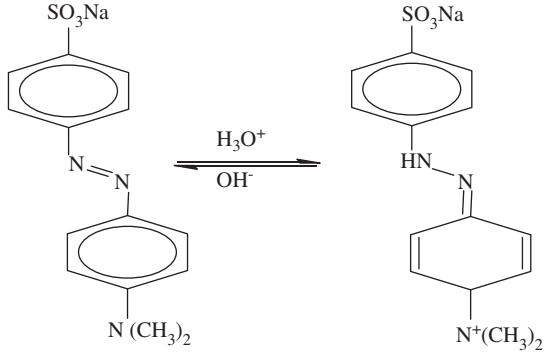

Fig. 9. Two forms of MO at acid and alkaline conditions.

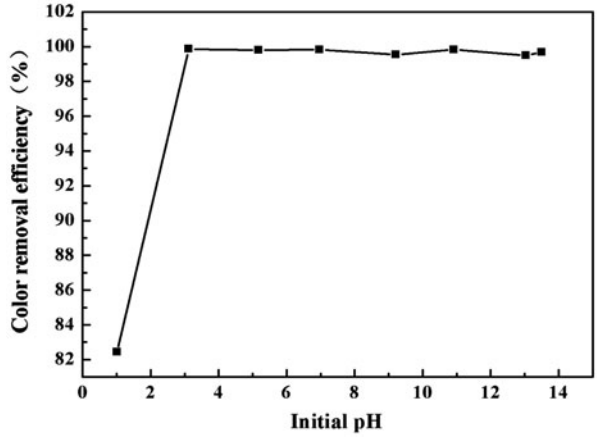

Fig. 10. Effect of initial pH on color removal efficiency.

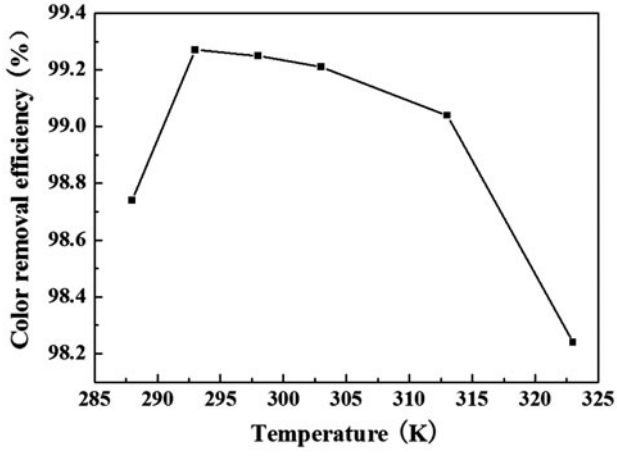

Fig. 11. Effect of contact temperature on color removal efficiency.

When pH > 3, the color removal efficiency remained almost unchanged (>99.5%), indicating that Al/CTAB-bent has a wide range of applications.

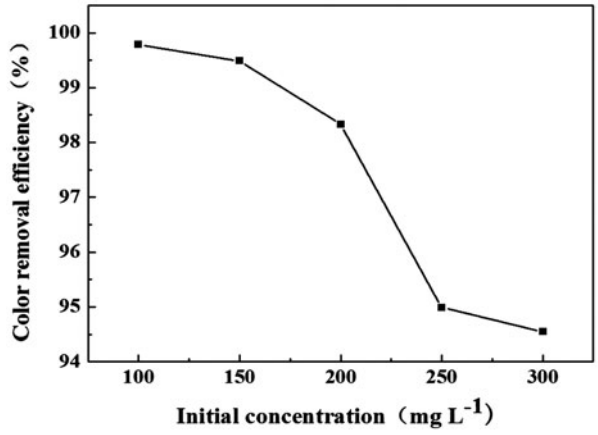

Fig. 12. Effect of initial concentration of MO on color removal efficiency.

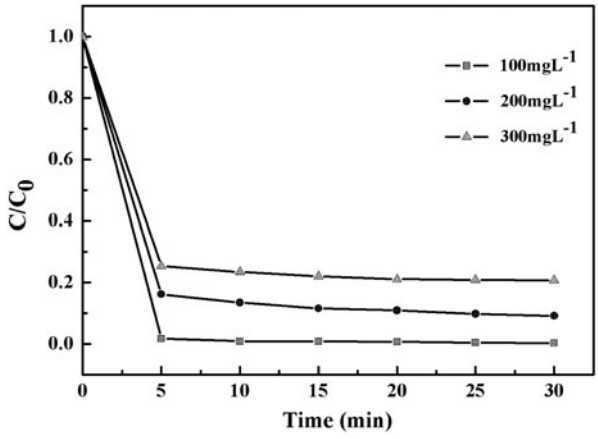

Fig. 13. The kinetics of MO adsorption onto Al/CTAB-bent at various initial concentrations.

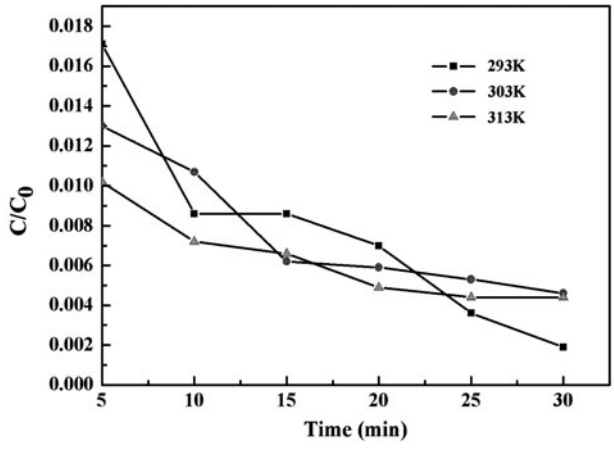

Fig. 14. The kinetics of MO adsorption onto Al/CTAB-bent at various temperatures.

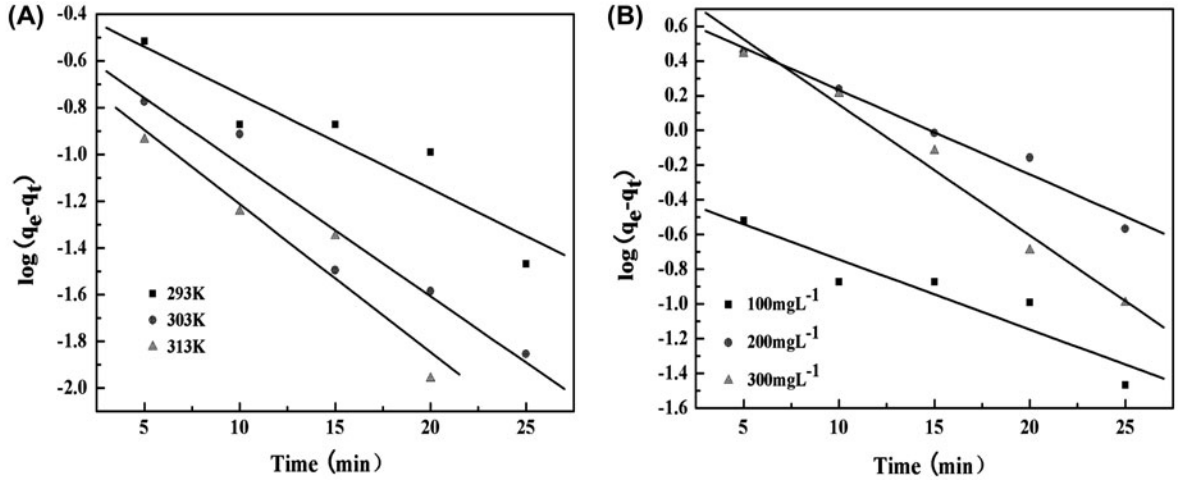

Fig. 15. The pseudo-first-order kinetics plots for the adsorption of MO onto Al/CTAB-bent at (A) various temperatures and (B) various MO initial concentrations.

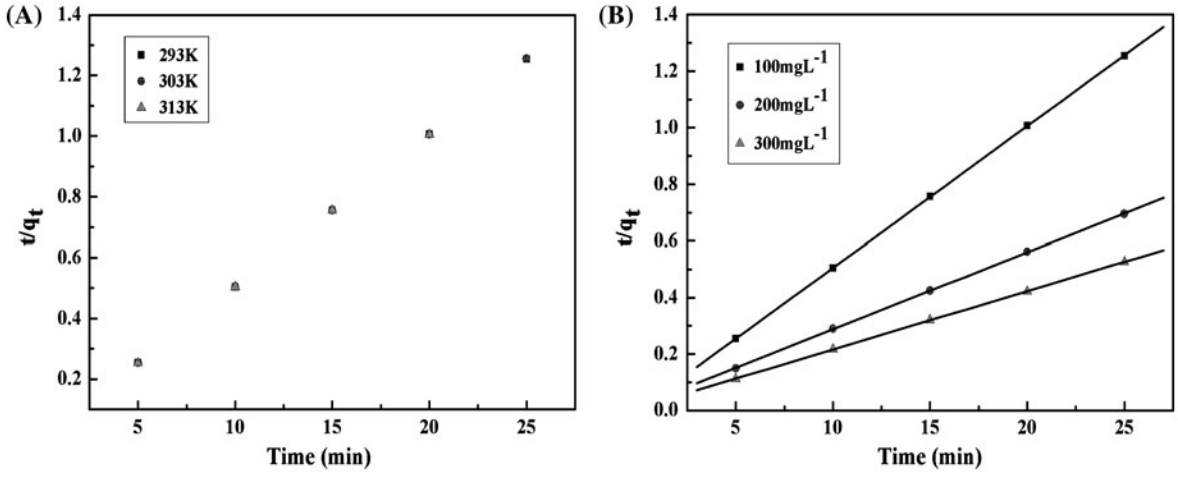

Fig. 16. The pseudo-second-order kinetics plots for the adsorption of MO onto Al/CTAB-bent at (A) various temperatures and (B) various MO initial concentrations.

Table 4
The pseudo-first-order and pseudo-second-order kinetics parameters for the adsorption of MO onto Al/CTAB-bent

T (K)	c_0 (mgL^{-1})	$q_{e,exp}$ (mgg^{-1})	Pseudo-first-order			Pseudo-second-order		
			q_e (mgg^{-1})	k_1 (min^{-1})	r_1^2	q_e (mgg^{-1})	k_2 (g mg^{-1}min^{-1})	r_2^2
293	100	19.96	0.4590	0.0930	0.8698	19.96	0.5705	0.9999
	200	36.25	5.2324	0.1119	0.9754	36.63	0.04871	0.9999
	300	47.55	8.0057	0.1736	0.9787	48.31	0.04674	0.9999
303	100	19.92	0.3346	0.1303	0.944	19.96	0.8367	0.9999
313	100	19.91	0.2641	1.3318	0.972	19.92	1.3264	0.9999

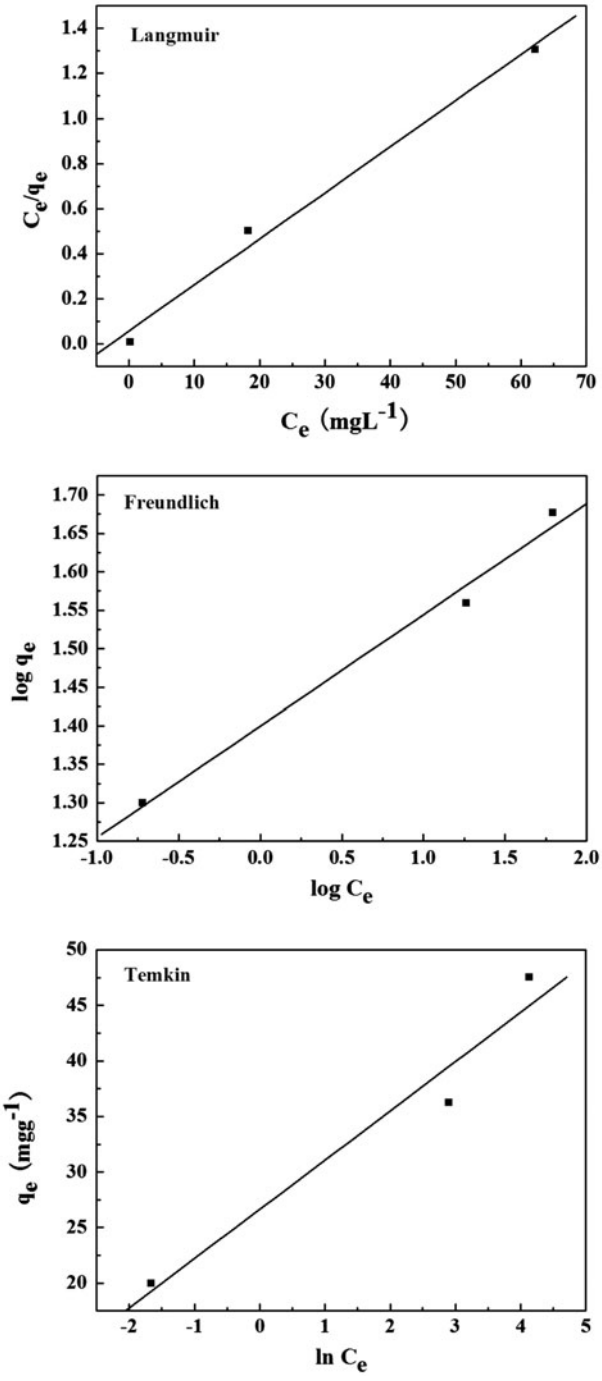

Fig. 17. Langmuir, Freundlich, and Temkin adsorption isotherm of MO adsorption onto Al/CTAB-bent at 293 K.

3.2.5. Effect of temperature on adsorption

Generally, many processes are affected by the temperature [43]. In the same conditions, the influence of temperature (288–323 K) on the color and COD removal efficiency of MO was investigated and the results are shown in Fig. 11.

The optimum temperature was chosen as 293 K. It can be assumed that the adsorption of MO onto Al/CTAB-bent is exothermic in nature. Similar results have been reported for the adsorption behavior of a textile dye of Reactive Blue 19 from aqueous solutions onto modified bentonite [27].

3.2.6. Effect of MO initial concentration on adsorption

Fig. 12 shows the effect of MO initial concentration on the removal of MO by Al/CTAB-bent. Theoretically, increasing the initial MO concentration would increase the mass transfer driving force and the rate of MO molecules passing from the bulk solution to the particle surface, resulting in higher MO adsorption and removal. However, the removal of MO decreases relatively as the initial MO concentration increases. It can be seen that as the initial MO concentration increased from 100 to 300 mg L^{-1}, the color removal efficiency decreased from 99.77 to 82.42%.

3.3. Adsorption kinetics

The effect of the initial concentration and temperature on the kinetics of MO uptake by Al/CTAB-bent is shown in Figs. 13 and 14. The relatively high MO removal is attributed to the availability of a large number of vacant sites on the surface of Al/CTAB-bent for MO adsorption [44,45]. The removal increases with the decrease of initial dye concentration when the adsorbent dosage is constant. A slight higher MO removal for higher temperature (313 K) than moderate temperature (293 K and 303 K) at the first 10 min, with longer time (30 min), the highest removal was observed at 293 K (Fig. 14). These results show that these adsorption reactions were complex and appeared to have a favorable adsorption at room temperature.

Table 5
Adsorption parameters for MO onto Al/CTAB-bent at 293 K

Langmuir				Freundlich			Temkin		
q_{max} (mg g^{-1})	R^2	K_L (L mg^{-1})	R_L	K_F	n	R^2	A	B	R^2
49.02	0.9902	0.36	0.0092–0.027	25.10	6.91	0.9883	26.64	4.44	0.9543

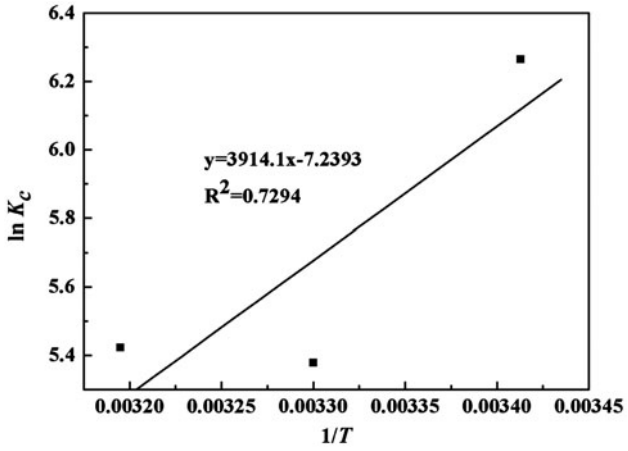

Fig. 18. Plot of $\ln K_c$ vs. $1/T$ for MO adsorption onto Al/CTAB-bent.

The kinetics data obtained using the pseudo-first and pseudo-second model are depicted in Figs. 15 and 16, respectively. The parameters k, q_e, and R^2 were calculated and are shown in Table 4. The r^2 of the pseudo-first-order model are lower than those of the pseudo-second-order model, and the calculated q_e appeared to be much close to the experimental values, indicating that pseudo-second-order model yields a better fit to the experimental data than the pseudo-first-order model. Similar results have been reported for the biosorbent for tungsten [46].

Table 6
Thermodynamic parameters for the adsorption of MO onto Al/CTAB-bent

T (K)	K_c	ΔG_0 (kJ mol^{-1})	ΔH_0 (kJ mol^{-1})	ΔS_0 (J mol^{-1} K^{-1})
293	525.32	−16.18	−32.54	−60.19
303	216.39	−13.55		
313	226.27	−14.11		

Table 7
Comparison of the adsorption capacity for various adsorbents in MO removal

Adsorbent	Maximum adsorption capacity, Q_0 (mg g^{-1})	Ref.
Hypercrosslinked polymer	76.92	[50]
Chitosan	34.83	[51]
Carbon nanotubes	35.4–64.7	[52]
Al/CTAB-bent	42.37–47.55	Present study

3.4. Adsorption isotherm

Fig. 17 shows adsorption isotherm of MO onto Al/CTAB-bent at 293 K. The values of q_{max}, K_L, K_F, n, A, and B and the correlation coefficients for Langmuir, Freundlich and for Temkin are given in Table 5. Based on the correlation coefficient, Langmuir equation represents a better fit of experimental data than Freundlich, indicating that the surface of Al/CTAB-bent is mainly made up of homogeneous adsorption patches.

The essential characteristics of the adsorption process can be determined by the separation factor R_L in the analysis of data by Langmuir isotherm, which is defined as:

$$R_L = \frac{1}{1 + K_L c_0} \tag{14}$$

R_L values indicate the shape of isotherm. The calculated values of R_L were found to be between 0 and 1 (0.0087–0.026), indicating that the adsorption of MO onto Al/CTAB-bent is favorable [47].

3.5. Thermodynamic of the adsorption process

The thermodynamic parameters are listed in Table 6. K_c indicates the capability of the bentonite to retain a solute and also the extent of its movement in a solution phase [48]. As shown in Table 6, K_c decreased with the temperature increasing from 293 to 323 K. The negative values of ΔG_0 at different temperatures indicate the feasibility of the process and the spontaneous nature of the adsorption. The ΔH_0 calculated from the slope of the line (Fig. 18) is −34.77 kJ mol^{-1}; the negative value indicates that the adsorption of MO onto Al/CTAB-bent was exothermic. Furthermore, higher negative ΔS_0 of MO adsorption process clearly state that the randomness decreased the Al/CTAB-bent-solution interface during adsorption [49].

Compared with other low-cost adsorbents for MO removal on the basis of their adsorption capacity, the adsorbent prepared in this study has higher adsorption capacity (Table 7 and 42.37–47.55 mg g^{-1} (0.1294 zmmol g^{-1})).

4. Conclusions

In this study, a modified bentonite, Al/CTAB-bent, was applied to remove MO from water. The color removal efficiency of 100 mg L^{-1} MO can reach above 99% and the COD removal efficiency above 97%. The

contact time, adsorbent dosage, temperature, pH, dye concentration, adsorption isotherms, adsorption kinetics, and adsorption thermodynamics were also examined. Optimal conditions for the adsorption of $100\,mg\,L^{-1}$ MO onto the Al/CTAB-bent were as follows: contact time of 30 min, $5\,g\,L^{-1}$ adsorbent, temperature of 293 K, and pH > 3. The kinetics data agree well with the pseudo-second-order kinetics model and the Langmuir adsorption isotherm model. And the adsorption thermodynamics indicate that the adsorption of MO onto the Al/CTAB-bent is spontaneous and exothermic. From the above discussion, it maybe concluded that the prepared adsorbent could be applied in industry wastewater treatment.

Acknowledgments

The authors are grateful to be supported by the Fundamental Research Funds for the Central Universities (GK201302013) and open fund (OGL201202) of State Key Laboratory of Organic Geochemistry, Guangzhou Institute of Geochemistry, Chinese Academy of Sciences, Guangzhou, China.

References

[1] Z.N. Liu, A.N. Zhou, G.R. Wang, X.G. Zhao, Adsorption behavior of methyl orange onto modified ultrafine coal powder, Chin. J. Chem. Eng. 17(6) (2009) 942–948.
[2] T.K. Saha, N.C. Bhoumik, S. Karmaker, M.G. Ahmedl, H. Ichikawa, Y. Fukumori, Adsorption of methyl orange onto chitosan from aqueous solution, J. Water Resour. Protect. 2 (2010) 898–906.
[3] H.E. Boujaady, A.E. Rhilassi, M. Bennani-Ziatni, R.E. Hamri, A. Taitai, J.L. Lacout, Removal of a textile dye by adsorption on synthetic calcium phosphates, Desalination 275 (2011) 10–16.
[4] B.P. Dojcinovi, G.M. Rogli, B.M. Obradovi, M.M. Kuraicac, M. M. Kosti, J. Nesi, D.D. Manojlovi, Decolorization of reactive textile dyes using water falling film dielectric barrier discharge, J. Hazard. Mater. 192 (2011) 763–771.
[5] A.A. Khan, Q. Husain, Potential of plant polyphenol oxidases in the decolorization and removal of textile and non-textile dyes, J. Environ. Sci. 19 (2007) 396–402.
[6] G. Crini, Non-conventional low-cost adsorbents for dye removal: A review, Bioresour. Technol. 97 (2006) 1061–1085.
[7] N. Panda, H. Sahoo, S. Mohapatra, Decolourization of methyl orange using Fenton-like mesoporous FeO–SiO composite, J. Hazard. Mater. 185 (2011) 359–365.
[8] M.H. Gehlen, M. Ferreira, M.G. Neumann, Interaction of methyl orange with cationic micelles and its effect on dye photochemistry, J. Photochem. Photobiol., A 87 (1995) 55–60.
[9] E.N.E. Qada, S.J. Allen, G.M. Walker, Adsorption of basic dyes from aqueous solution onto activated carbons, Chem. Eng. J. 135 (2008) 174–184.
[10] V.K. Gupta, A. Mittal, L. Kurup, J. Mittal, Adsorption of a hazardous dye, erythrosine, over hen feathers, J. Colloid Interface Sci. 304 (2006) 52–57.
[11] V.K. Gupta, A. Rastogi, A. Nayak, Biosorption of nickel onto treated alga (Oedogonium hatei): Application of isotherm and kinetic models, J. Colloid Interface Sci. 342 (2010) 533–539.
[12] I.D. Mall, V.C. Srivastava, N.K. Agarwal, Removal of orange-G and methyl violet dyes by adsorption onto bagasse fly ash-dkinetic study and equilibrium isotherm analyses, Dyes Pigm. 69 (2006) 210–223.
[13] V.K. Gupta, B. Gupta, A. Rastogi, S. Agarwal, A. Nayak, Pesticides removal from waste water by activated carbon prepared from waste rubber tire, Water Res. 45 (2011) 4047–4055.
[14] V.K. Gupta, B. Gupta, A. Rastogi, S. Agarwal, A. Nayak, A comparative investigation on adsorption performances of mesoporous activated carbon prepared from waste rubber tire and activated carbon for a hazardous azo dye-acid blue 113, J. Hazard. Mater. 186 (2011) 891–901.
[15] V.K. Gupta, A. Mittal, A. Malviya, J. Mittal, Adsorption of carmoisine A from wastewater using waste materials-bottom ash and deoiled soya, J. Colloid Interface Sci. 335 (2009) 24–33.
[16] A. Mittal, J. Mittal, A. Malviya, D. Kaur, V.K. Gupta, Adsorption of hazardous dye crystal violet from wastewater by waste materials, J. Colloid Interface Sci. 343 (2010) 463–473.
[17] A. Mittal, L. Kurup (Krishnan), V.K. Gupta, Use of waste materials-bottom ash and de-oiled soya, as potential adsorbents for the removal of Amaranth from aqueous solutions, J. Hazard. Mater. B117 (2005) 171–178.
[18] V.K. Gupta, A. Mittal, V. Gajbe, J. Mittal, Removal and recovery of the hazardous azo dye acid orange 7 through adsorption over waste materials: Bottom ash and de-oiled soya, Ind. Eng. Chem. Res. 45 (2006) 1446–1453.
[19] V.K. Gupta, A. Rastogi, A. Nayak, Adsorption studies on the removal of hexavalent chromium from aqueous solution using a low-cost fertilizer industry waste material, J. Colloid Interface Sci. 342 (2010) 135–141.
[20] V.K. Gupta, I. Ali, V.K. Saini, Defluoridation of wastewaters using waste carbon slurry, Water Res. 41 (2007) 3307–3316.
[21] V.K. Gupta, R. Jain, S. Malathi, A. Nayak, Adsorption-desorption studies of indigocarmine from industrial effluents by using deoiled mustard and its comparison with charcoal, J. Colloid Interface Sci. 348 (2010) 628–633.
[22] V.K. Gupta, A. Nayak, Cadmium removal and recovery from aqueous solutions by novel adsorbents prepared from orange peel and Fe_2O_3 nanoparticles, Chem. Eng. J. 180 (2012) 81–90.
[23] V.K. Gupta, R. Jain, S. Varshney, Removal of Reactofix golden yellow 3 RFN from aqueous solution using wheat husk: An agricultural waste, J. Hazard. Mater. 142 (2007) 443–448.
[24] Z.X. Chen, X.Y. Jin, Z.L. Chen, M. Megharaj, R. Naidu, Removal of methyl orange from aqueous solution using bentonite-supported nanoscale zero-valent iron, J. Colloid Interface Sci. 363 (2011) 601–607.
[25] F.G.E. Nogueira, J.H. Lopes, A.C. Silva, M. Gonçalves, A.S. Anastácio, K. Sapag, L.C.A. Oliveira, Reactive adsorption of methylene blue on montmorillonite via an ESI-MS study, Appl. Clay Sci. 43 (2009) 190–195.
[26] M.Y. Teng, S.H. Lin, Removal of methyl orange dye from water onto raw and acid activated montmorillonite in fixed beds, Desalination 201 (2006) 71–81.
[27] O. Gok, A.S. Ozcan, A. Ozcan, Adsorption behavior of a textile dye of Reactive Blue 19 from aqueous solutions onto modified bentonite, Appl. Surf. Sci. 256 (2010) 5439–5443.
[28] J.F. Ma, L.Z. Zhu, Simultaneous sorption of phosphate and phenanthrene to inorgano-organo-bentonite from water, J. Hazard. Mater. B136 (2006) 982–988.
[29] S.B. Wang, H.W. Wu, Environmental-benign utilization of fly ash as low-cost adsorbents, J. Hazard. Mater. 136 (2006) 482–501.
[30] S. Azizian, Kinetic models of sorption: A theoretical analysis, J. Colloid Interface Sci. 276 (2004) 47–52.
[31] A.K. Rahardjo, M.J.J. Susanto, A. Kurniawan, N. Indraswati, S. Ismadji, Modified Ponorogo bentonite for the removal of ampicillin from wastewater, J. Hazard. Mater. 190 (2011) 1001–1008.

[32] Y.C. Wong, Y.S. Szeto, W.H. Cheung, G. McKay, Equilibrium studies for acid dye adsorption onto chitosan, Langmuir 19 (2003) 7888–7894.
[33] X.D. Xin, W. Si, Z.X. Yao, R. Feng, B. Dua, L.G. Yan, Q. Wei, Adsorption of benzoic acid from aqueous solution by three kinds of modified bentonites, J. Colloid Interface Sci. 359 (2011) 499–504.
[34] H. Chen, A.Q. Wang, Kinetic and isothermal studies of lead ion adsorption onto palygorskite clay, J. Colloid Interface Sci. 307 (2007) 309–316.
[35] N. Babakhouya, H. Aksas, S. Boughrara, K. Louhab, Adsorption of Cd(II) Ions from aqueous solution using mixed sorbents prepared from olive stone and date pit, J. Appl. Sci. 10 (19) (2010) 2316–2321.
[36] D. Tiwari, C. Laldanwngliana, C.H. Choi, S.M. Lee, Manganese-modified natural sand in the remediation of aquatic environment contaminated with heavy metal toxic ions, Chem. Eng. J. 171 (2011) 958–966.
[37] B. Zohra, K. Aicha, S. Fatima, B. Nourredine, D. Zoubir, Adsorption of direct red 2 on bentonite modified by cetyltrimethylammonium bromide, Chem. Eng. J. 136 (2008) 295–305.
[38] X.J. Huang, S.M. Xu, M. Zhong, J.D. Wang, S. Feng, R.F. Shi, Modification of Na-bentonite by polycations for fabrication of amphoteric semi-IPN nanocomposite hydrogels, Appl. Clay Sci. 42 (2009) 455–459.
[39] E. Alver, A.Ü. Metin, Anionic dye removal from aqueous solutions using modified zeolite: Adsorption kinetics and isotherm studies, Chem. Eng. J 200–202 (2012) 59–67.
[40] Z. Liu, X. Yan, M. Drikas, D. Zhou, D. Wang, M. Yang, J. Qu, Removal of bentazone from micro-polluted water using MIEX resin: Kinetics, equilibrium, and mechanism, J. Environ. Sci. 23 (2011) 381–387.
[41] L.L. Lian, L.P. Guo, C.J. Guo, Adsorption of congo red from aqueous solutions onto Ca-bentonite, J. Hazard. Mater. 161 (2009) 126–131.
[42] H.Z. Ma, B. Wang, X.Y. Luo, Studies on degradation of methyl orange wastewater by combined electrochemical process, J. Hazard. Mater. 149 (2007) 492–492.
[43] Y.H. Liou, S.L. Lo, C.J. Lin, W.H. Kuan, S.C. Weng, Chemical reduction of an unbuffered nitrate solution using catalyzed and uncatalyzed nanoscale iron particles, J. Hazard. Mater. B127 (2005) 102–110.
[44] D.S. Sun, X.D. Zhang, Y.D. Wu, X. Liu, Adsorption of anionic dyes from aqueous solution on fly ash, J. Hazard. Mater. 181 (2010) 335–342.
[45] Q.H. Hu, S.Z. Qiao, F. Haghseresht, M.A. Wilson, G.Q. Lu, Adsorption study for removal of basic red dye using bentonite, Ind. Eng. Chem. Res. 45 (2006) 733–738.
[46] H. Gecol, E. Ergican, P. Miakatsindila, Biosorbent for tungsten species removal from water: effects of co-occurring inorganic species, J. Colloid Interface Sci. 292 (2005) 344–353.
[47] C. Namasivayam, D. Kavitha, Removal of congo red from water by adsorption onto activated carbon prepared from coir pith, an agricultural solid waste, Dyes Pigm. 54 (2002) 47–58.
[48] E. Eren, B. Afsin, Investigation of a basic dye adsorption from aqueous solution onto raw and pretreated bentonite surfaces, Dyes Pigm. 73 (2007) 162–167.
[49] M. Alkan, O. Demirbas, S. Celikcapa, M. Dogan, Sorption of acid red 57 from aqueous solution onto sepiolite, J. Hazard. Mater. B116 (2004) 135–145.
[50] J.H. Huang, K.L. Huang, S.Q. Liu, A.T. Wang, Ch. Yan, Adsorption of rhodamine B and methyl orange on a hypercrosslinked polymeric adsorbent in aqueous solution, Colloids Surf., A 330 (2008) 55–61.
[51] T.K. Saha, N.C. Bhoumik, S. Karmaker, M.G. Ahmed, H. Ichikawa, Y. Fukumori, Adsorption of methyl orange onto chitosan from aqueous solution, J. Water Resour. Protect. 2 (2010) 898–906.
[52] Y.J. Yao, B. He, F.F. Xu, X.F. Chen, Equilibrium and kinetic studies of methyl orange adsorption on multiwalled carbon nanotubes, Chem. Eng. J. 170 (2011) 82–89.